Mesostructure of Anatase Thin Films Prepared by Mesophase Templating

Florence Bosc,*,† André Ayral,† Pierre-Antoine Albouy,‡ Lucien Datas,§ and Christian Guizard†

Institut Européen des Membranes, UMR no. 5635, CNRS-ENSCM-UMII, CC047, Université Montpellier II, F-34095 Montpellier Cedex 5, France, Laboratoire de Physique des Solides, UMR no. 8502, CNRS-Université Paris-Sud XI, Bât. 510, Université Paris-Sud, F-91405 Orsay, France, and CIRIMAT, UMR no. 5085, CNRS-UPS-INPT, Université Paul Sabatier, Bât. 3R1B3, 118 Route de Narbonne, F-31062 Toulouse Cedex 4, France

Received January 19, 2004. Revised Manuscript Received March 16, 2004

A previous paper described the low-temperature synthesis of mesoporous nanocrystalline anatase thin layers obtained by mesophase templating (*Chem. Mater.* **2003**, *15*, 2463). This work deals with the structural characterization of these anatase thin layers and with the extension of the synthesis method to films with a different mesostructure. Thus, two triblock copolymers are used as structuring agents and the effect of the volume fraction of surfactant in the dried layers is also considered. The determination of the mesostructures is mainly based on 2D X-ray diffraction experiments, completed with observations by transmission electron microscopy and atomic force microscopy. Nitrogen adsorption−desorption measurements are performed to investigate the porous texture of the thin layers.

Introduction

Preparation of nanocrystalline anatase TiO_2 thin films opens important perspectives for a number of technological applications such as photovoltaic cells, self-cleaning panels, and electrochemical sensors or for photocatalyzed reactions.[1−14] In addition to the intrinsic photoactivity which is directly related to the nanometric size of the anatase crystals, the accessibility of the chemical species to the pore surface strongly depends on the porous characteristics of the anatase layers. An attractive method to obtain an ordered mesoporosity is the use of the templating effect of lyotropic mesophases resulting from the self-assembly of amphiphilic molecules such as triblock copolymers.[15−21] In a recent paper,[1] the feasibility at low temperature of nanocrystalline anatase layers with an ordered mesoporosity has been demonstrated. According to the corresponding water−surfactant binary diagram,[22] a 2 D hexagonal structure ($p6mm$) was predicted.[1] The mesostructure of the layers is here precisely defined. The influence of the volume fraction of the surfactant in the dried layer is also considered. In parallel, the extension of the synthesis method to the preparation of layers with a cubic mesostructure is studied by using another triblock copolymer known to form a cubic mesophase with water.[20,21] In the amphiphilic media, it is possible to evidence different types of cubic mesophases:[23,24] micellar cubic phases resulting from the close-packing of spherical micelles ($Fm3m$, $Fd3m$)[23] or bicontinuous cubic based on micellar interconnected networks ($Im3m$, $Pn3m$, $Ia3d$).[24,25] The bicontinuous cubic mesophases are

* To whom correspondence should be addressed. Tel: 33-4-67-14-91-58. Fax: 33-4-67-14-91-19. E-mail: Florence.Bosc@iemm.univ-montp2.fr.

† Université Montpellier II.

‡ Université Paris-Sud.

§ Université Paul Sabatier.

(1) Bosc, F.; Ayral, A.; Albouy, P.-A.; Guizard, C. *Chem. Mater.* **2003**, *15*, 2463.

(2) Fujishima, A., Hashimoto, K., Watanabe, T., Eds. *TiO_2 Photocatalysis, Fundamentals and Applications*; BKC, Inc.: Tokyo, 2001; p 176.

(3) Richards, B. S.; Rowlands, S. F.; Ueranatasun, A.; Cotter, J. E.; Honsberg, C. B. *Solar Energy* **2003**, *76*, 269.

(4) Miyairi, K.; Itoh, E.; Hashimoto, Y. *Thin Solid Films* **2003**, *438−439*, 147.

(5) Boyle, D. S.; Govender, K.; O'Brien, P. *Thin Solid Films* **2003**, *431−432*, 483.

(6) Mills, A.; Hill, G.; Bhopal, S.; Parkin, I. P.; O'Neill, S. A. *J. Photochem. Photobiol,. A* **2003**, *160*, 185.

(7) Yamashita, H.; Nakao, H.; Takeuchi, M.; Nakatani, Y.; Anpo, M. *Nucl. Instrum. Methods Phys. Res., Sect. B* **2003**, *206*, 898.

(8) Puzenat, E.; Pichat, P. *J. Photochem. Photobiol., A* **2003**, *160*, 127.

(9) Mills, A.; Lepre, A.; Elliott, N.; Bhopal, S.; Parkin, I. P.; O'Neill, S. A. *J. Photochem. Photobiol., A* **2003**, *160*, 213.

(10) Kumazawa, N.; Rafiqul Islam, M.; Takeuchi, M. *J. Electroanal. Chem.* **1999**, *472*, 137.

(11) Rafiqul Islam, M.; Kumazawa, N.; Takeuchi, M. *Sens. Actuators, B* **1998**, *46*, 114.

(12) Anpo, M.; Takeuchi, M. *J. Catal.* **2003**, *216*, 505.

(13) Pichat, P.; Disdier, J.; Hoang-Van, C.; Mas, D.; Goutailler, G.; Gaysse, C. *Catal. Today* **2000**, *63*, 363.

(14) Molinari, R.; Grande, C.; Drioli, E.; Palmisano, L.; Schiavello, M. *Catal. Today* **2001**, *67*, 273.

(15) Huo, Q.; Margolese, D. I.; Ciesla, U.; Demuth, D. G.; Feng, P.; Gier, T. E.; Sieger, P.; Firouzi, A.; Chmelka, B. F.; Schüth, F.; Stucky, G. D. *Chem. Mater.* **1994**, *6*, 1176.

(16) Klotz, M.; Ayral, A.; Guizard, C.; Cot, L. *Bull. Korean Chem. Soc.* **1999**, *20*, 879.

(17) Yang, P.; Zhao, D.; Margolese, D. I.; Chmelka, B. F.; Stucky, G. D. *Nature* **1998**, *396*, 152.

(18) Grosso, D.; Soler-Illia, G. J. d. A. A.; Crepaldi, E. L.; Cagnol, F.; Sinturel, C.; Bourgeois, A.; Brunet-Bruneau, A.; Amenitsch, H.; Albouy, P.-A.; Sanchez, C. *Chem. Mater.* **2003**, *15*, 4562.

(19) Crepaldi, E. L.; Soler-Illia, G. J. d. A. A.; Grosso, D.; Cagnol, F.; Ribot, F.; Sanchez, C. *J. Am. Chem. Soc.* **2003**, *125*, 9770.

(20) Klotz, M.; Idrissi-Kandri, N.; Ayral, A.; Guizard, C. *Mater. Res. Soc.* **2000**, *628*, 7.4.1

(21) Crepaldi, E. L.; Soler-Illia, G. J. d. A. A.; Grosso, D.; Albouy, P.-A.; Sanchez, C. *Chem. Commun.* **2001**, 1582.

(22) Wanka, G.; Hoffmann, H.; Ulbrich, W. *Macromolecules* **1994**, *27*, 4145.

(23) Borisch, K.; Diele, S.; Göring, P.; Kresse, H.; Tschierske, C. *J. Mater. Chem.* **1998**, *8*, 529.

(24) Clerc, M. Etude de transition de phase vers les phases cubiques des systèmes eau/surfactant., Ph.D. Thesis, Université Paris XI Orsay, France, 1992.

10.1021/cm049893a CCC: $27.50
Published on Web 04/24/2004

expected to generate isotropic and interconnected mesoporous networks. From this point of view, they are attractive for applications such as separative membranes.[26,27] The mesostructures usually observed for mesoporous TiO_2 obtained by mesophase templating exhibit the same centered cubic space group, $Im3m$.[18,19,28−30]

Experimental Section

Anatase Sol Synthesis. The starting anatase hydrosol was synthesized from titanium isopropoxide hydrolyzed in acidic conditions as previously described.[1] After aging for 3 h at 30 °C, anatase nanoparticles with a mean hydrodynamic radius of 6 nm were obtained. The structuring agent was then introduced in the sol. The amphiphilic molecules used were triblock copolymers poly(ethylene oxide)−poly(propylene oxide)−poly(ethylene oxide): $EO_{20}PO_{70}EO_{20}$ and $EO_{106}PO_{70}EO_{106}$, labeled P_{123} and F_{127}, respectively, and provided by BASF. To compare the domains of existence of the ordered layers with the domain of formation of the corresponding mesophases in the water−surfactant binary diagram, the volume fraction of surfactant in the dried layer (Φ_v) is a pertinent parameter.[31,32] The investigated range of Φ_v was from 50 to 80%. The nomenclature used to identify the synthesized thin layers will be as follows: PX or FX, with P or F defining the nature of the used copolymer, P_{123} or F_{127}, respectively, and with X being the volume fraction of surfactant (expressed in %). The two mainly studied compositions P70 (Φ_{P123} = 70%) and F67 (Φ_{F127} = 67%) correspond to films exhibiting the best characteristics in terms of mesostructure quality and of thermal stability.

Thin Layers Preparation. Thin films were deposited by dip-coating onto slides of soda lime−silica glass (withdrawal rate 5 cm·min^{-1}). After drying at room temperature under controlled humidity for 1 day (HR = 98%), the films were thermally treated at 150 °C for 2 days and then calcined to higher temperatures. In the case of samples PX, complete elimination of the templating units can be reached at low temperature if the thermal treatment at 150 °C is followed by photodegradation under UV irradiation (2 min; lamp power 280 W·m^{-2}). For the layers FX, a thermal treatment up to 350 °C is required for complete removal of the structuring agent.

Characterization. One-dimension X-ray diffraction (1D-XRD) measurements were performed with an X'pert-Pro (PanAnalytical) diffractometer, a $\theta/2\theta$ Bragg Brentano configuration, and the $K-L_{3,2}$ rays of copper. This apparatus is equipped with a furnace (Anton Paar HTK-1200) for analyses at high temperature. For the experiments on the thermal evolution of the structure, the heating rate was 5 °C·min^{-1}, with a stop each 25 °C, and a dwell of 10 min before recording the X-ray pattern. For the other thermal treatments, the heating rate was 1 min^{-1} with a dwell of 3 h at the final temperature. The mesostructure determination and the textural analysis of the layers were investigated using a two-dimensional X-ray diffraction device (2D-XRD) at grazing incidence. The experiments were carried out with a rotating anode X-ray generator, with the sample−detector distance being continuously adjustable. The scattered signal was recorded on photostimulable imaging plates. The layers were also characterized by transmission electron microscopy (TEM; JEOL JEM 2010). In that case, samples were prepared by scrapping the films from the substrate and by deposition of chips on copper grids. The morphological analysis of the surface of the thin layers was done using an atomic force microscope (AFM). The apparatus is a commercial Nanoscope IIIa (Digital Instruments) in the tapping mode. Silicon cantilevers with a pyramidal shape and a tip curvature radius smaller than 10 nm were used. The typical scan rate was around 1 Hz. Squared images were acquired at a digitalization rate comprised of between 256 and 512 points per line. The porous texture of the thin layers was investigated from nitrogen adsorption−desorption isotherms at 77 K, using a special cell designed for glass plates[33] and a volumetric apparatus (Micromeritics ASAP 2010). The BET[34] and BJH[35] methods were applied for determination of the specific surface area, S_{BET}, and of the mean mesopore equivalent diameter, respectively.

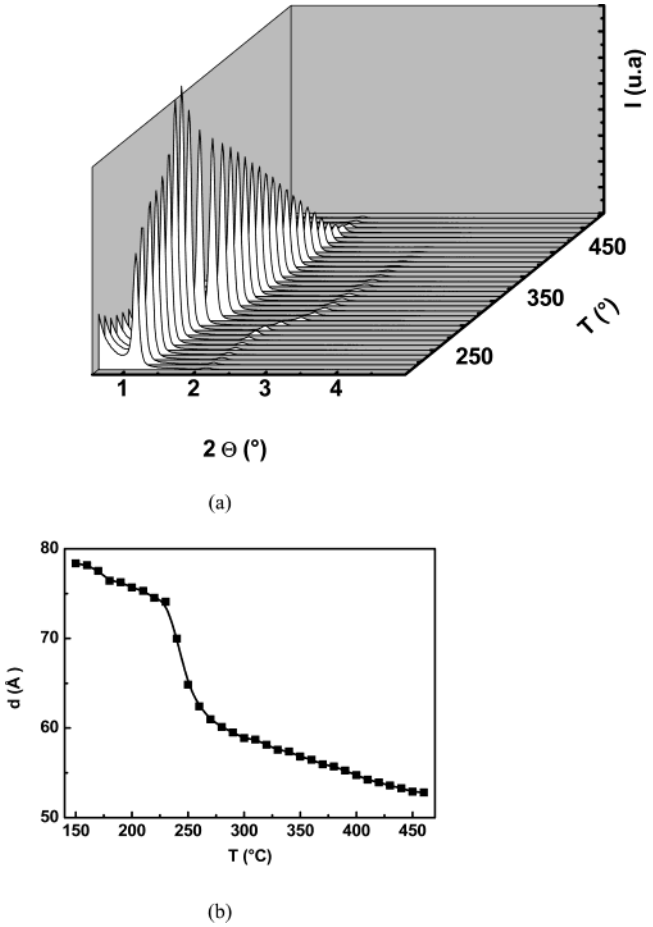

Figure 1. (a) Thermal evolution of the low-angle 1D-XRD pattern for layer P70. (b) Thermal evolution of the Bragg spacing for the main diffraction peak for sample P70.

Results and Discussion

Thin Layers of PX Type. The ordered mesostructure of sample P70 is clearly evidenced from its low-angle 1D-XRD pattern (Figure 1a), the ordered mesoporosity being maintained until 500 °C. The mesostructure disappearance is in fact associated with the crystalliza-

(25) Hyde, S. T. Identification of Lyotropic Liquid Crystalline mesophases. In *Handbook of Applied Surface and Colloid Chemistry*; Holmberg, K., Ed.; John Wiley & Sons: 2001; p 299.
(26) Schacht, S.; Huo, Q.; Voigt-Martin, I.; Stucky, G. D.; Schüth, F. *Science* **1996**, *273*, 768.
(27) McGrath, K. M.; Dabbs, D. M.; Yao, N.; Aksay, I. A.; Gruner, S. M. *Science* **1997**, *277*, 552.
(28) Crepaldi, E. L.; Soler-Illia, G. J. d. A. A.; Grosso, D.; Sanchez, C. *New J. Chem.* **2003**, *27*, 9.
(29) Alberius, P. C. A.; Frindell, K. L.; Hayward, R. C.; Kramer, E. J.; Stucky, G. D.; Chmelka, B. F. *Chem. Mater.* **2002**, *14*, 3284.
(30) Yang, P.; Zhao, D.; Margolese, D. I.; Chmelka, B. F.; Stucky, G. D. *Chem. Mater.* **1999**, *11*, 2813.
(31) Klotz, M.; Besson, S.; Ricolleau, C.; Bosc, F.; Ayral, A. *Mater. Res. Soc.* **2003**, *752*, AA8.6.1.
(32) Klotz, M.; Ayral, A.; Guizard, C.; Cot, L. *J. Mater. Chem.* **2000**, *10*, 663.
(33) Ayral, A.; El Mansouri, A.; Vieira, M.; Pilon, C. *J. Mater. Sci. Lett.* **1998**, *17*, 883.
(34) Brunauer, S.; Emmet, P. H.; Teller, E. *J. Am. Chem. Soc.* **1938**, *60*, 309.
(35) Barrett, E. P.; Joyner, L. G.; Halenda, P. P. *J. Am. Chem. Soc.* **1951**, *73*, 373.

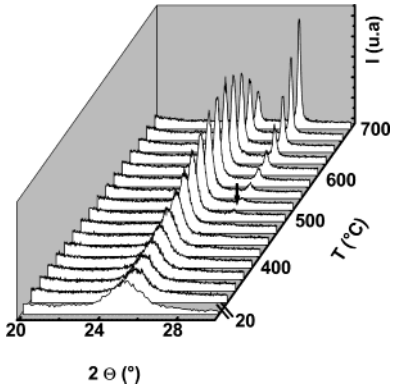

Figure 2. Thermal evolution of the large-angle 1D-XRD pattern for powder P70. (Black arrow: appearance of diffraction peak associated with rutile).

tion of the anatase walls into rutile as shown in Figure 2. Moreover a shift to larger angles of the main diffraction peak related to the ordered mesostructure is observed (Figure 1b). This shift, which corresponds to a reduction of the mesostructure lattice, mainly occurs around 250 °C. It can be associated with the departure of the structuring units (in the absence of UV treatment). The total shrinkage measured between 25 and 350 °C is around 25 ± 2%.

From the water−P_{123} binary diagram,[22] the expected mesostructure for the samples P70 is a 2D hexagonal structure resulting from a hexagonal close-packing of micellar cylinders. To experimentally determine the mesostructure symmetry and the texture of the layers, 2D-XRD experiments were performed (Figure 3). For the dried sample (Figure 3a), it is possible to index the diffraction spots with the *p*6*mm* space group in agreement with the expected 2D hexagonal structure. The presence of the diffraction spots in the grazing incidence pattern confirms the preferential parallel orientation of the micellar cylinders within the plane parallel to the surface of the films.[36] The thermal treatment of the layer P70 at 350 °C induces a modification of the 2D-XRD pattern (Figure 3b): the spots initially positioned on concentric circles are now located on ellipses. This phenomenon, which has been previously observed and

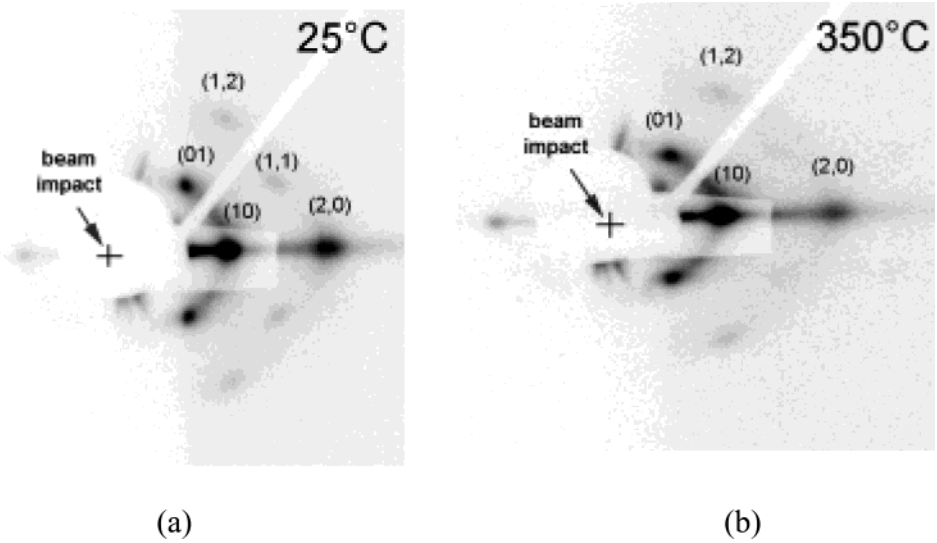

Figure 3. 2D-XRD patterns of layer P70: (a) dried at 25 °C, and (b) calcined at 350 °C.

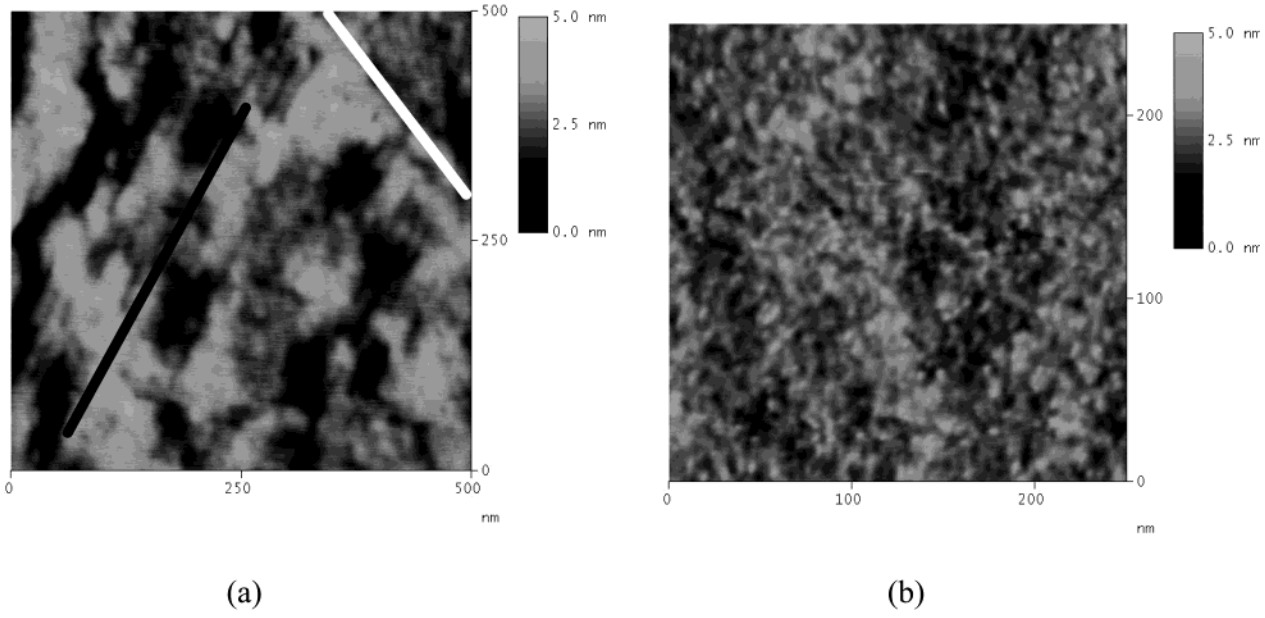

Figure 4. AFM images of the surface for (a) layer P70 treated at 350 °C, and (b) layer F67 treated at 350 °C.

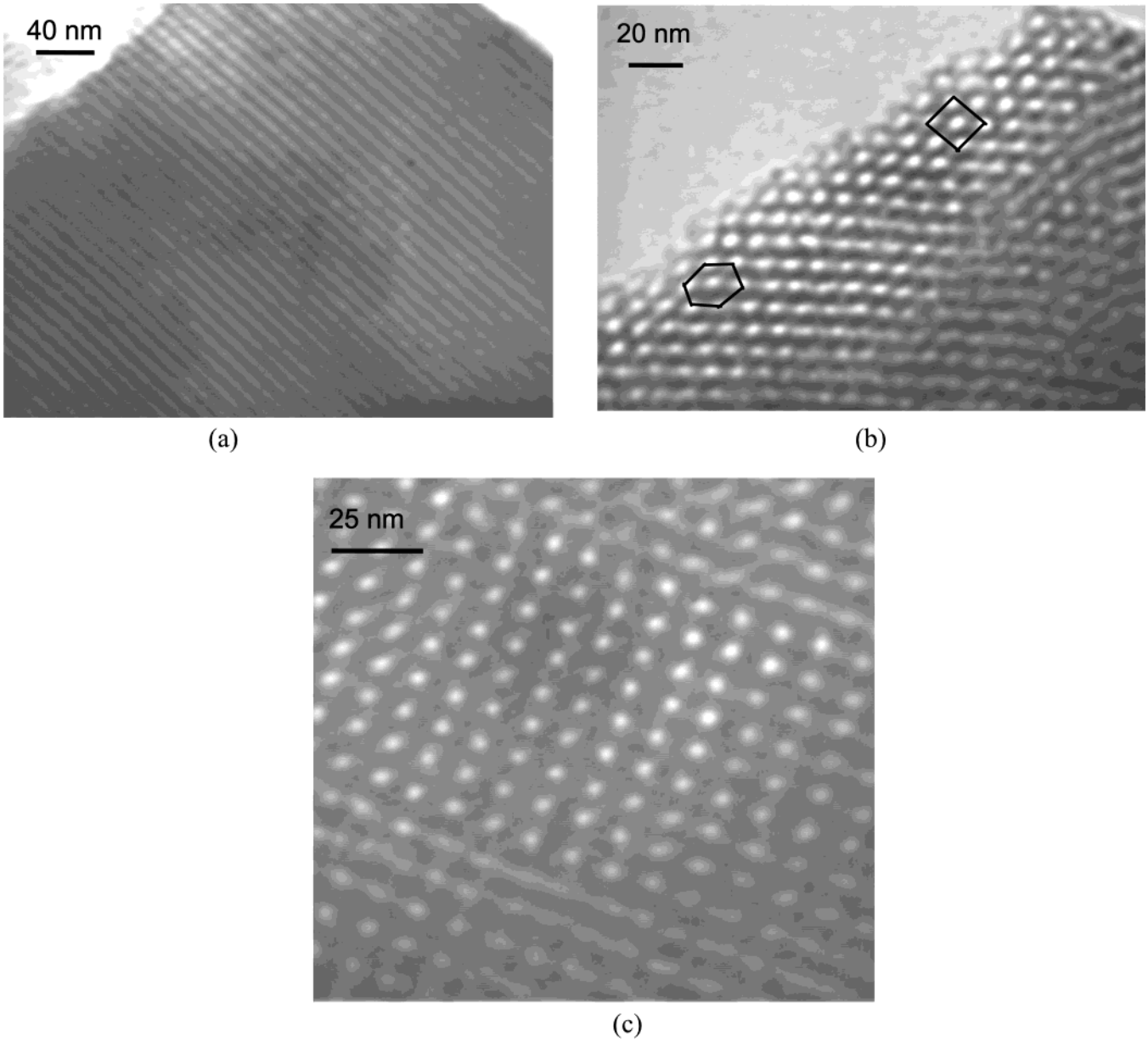

Figure 5. TEM images of chips obtained by scrapping thin layers calcined at 350 °C: (a) P70 within the plane of the pores, (b) P70 perpendicular to the plane of the pores with the schematic representations of the deformed 2D hexagonal lattice and of the rectangular lattice, and (c) F67.

detailed in the case of mesostructured silica layers,[36] is associated with a unidirectional shrinkage of the layer in the direction of the normal of the film. The resulting structure corresponds to the *c*2*mm* space group (rectangular symmetry). The shrinkage measured from the 2D-XRD pattern is around 22 ± 3%, in agreement with the value determined from the 1D-XRD data (the main diffraction peak observed on the 1D-XRD pattern corresponds to the planes (01) assuming a 2D hexagonal structure). The 2D-XRD pattern of the sample P70 treated at 350 °C also consists of spots due to a preferential orientation of the cylindrical pores within the plane parallel to the surface. From the 1D-XRD diffraction pattern of sample P70 treated at 350 °C (Figure 1a), the size of the ordered domains estimated from the width half-height maximum of the main diffraction peak using the Scherrer formula,[37] and assuming no structural distortion inside the ordered domains, is 200 ± 100 nm.

The AFM analysis of the surface of the layers P70 treated at 350 °C confirms the presence and the alignment of the cylindrical pores within the plane parallel to the surface. In Figure 4a, the black line symbolizes the direction of the alignment of the pores in an ordered domain, whereas the white line materializes the boundary between two ordered domains. Moreover, these observations confirm the order of magnitude previously determined for the size of the ordered domains, around a few hundred nanometers. The lattice parameter evaluated from the AFM image within the plane of the layer, 9 ± 1 nm, is also in agreement with the one determined from the 2D-XR pattern, 8.8 ± 0.2 nm.

Because of the sampling method, the TEM observations cannot be used to analyze the texture of the layers but only to confirm the structural data. Figure 5a and b show images of sample P70 treated at 350 °C. Similar images have been previously recorded with mesoporous silica obtained with P_{123} as structuring agent.[38] In

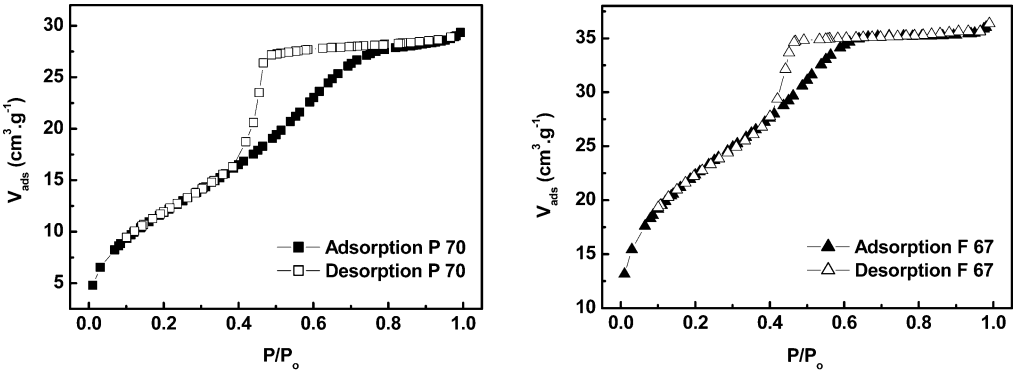

Figure 6. Nitrogen adsorption−desorption isotherms of layers treated at 350 °C: (a) P70, and (b) F 67.

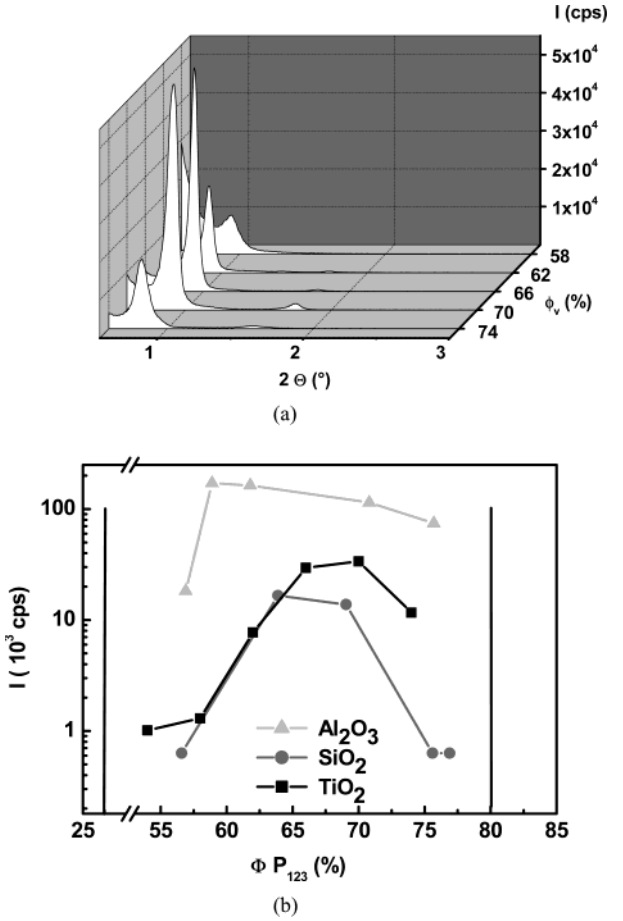

Figure 7. (a) Low-angle 1D-XRD pattern evolution versus Φ_V (P_{123}) for layers PX, and (b) evolution of the intensity of main diffraction peak as a function of Φ_V (P_{123}). The limits of the hexagonal phase at 30 °C in the water−P_{123} binary diagram are reported as vertical lines.

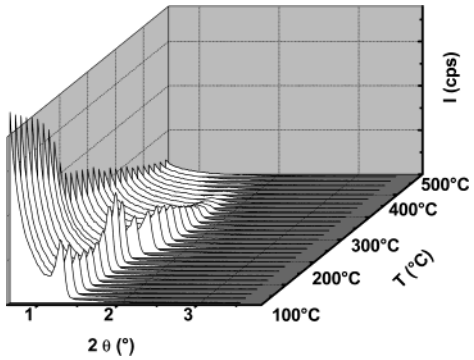

Figure 8. Thermal evolution of the low-angle 1D-XRD pattern for layer F67.

Figure 5a, the alignment of the cylindrical pores can be observed in an ordered domain about 400 nm in size. The deformation of the hexagonal structure into a rectangular one is confirmed in Figure 5b. The measured distance between the axes of the cylindrical pores is around 8 ± 1 nm, in agreement with the XRD and AFM measurements. The estimated pore diameter is 4 ± 1 nm.

The porosity of the layers P70 treated at 350 °C is investigated from the resulting nitrogen adsorption−desorption isotherm (Figure 6a). This type IV isotherm is typical of mesoporous materials.[39] A hysteresis loop is observed with dissimilar shapes for the adsorption and desorption branches unlike that predicted for cylindrical pores. This phenomenon was previously observed for different mesoporous oxides with cylindrical mesopores.[30,40] The abrupt drop on the desorption branch can be assigned to the presence of mesopore constrictions at the boundaries between the ordered domains and of smaller pores in the titania walls.[41] The mean cylindrical pore diameter determined from the adsorption branch using the BJH method is 4.2 ± 0.1 nm, in good agreement with the estimation from the TEM images (4 ± 1 nm). The BET specific surface area is equal to 190 ± 10 $m^2 \cdot g^{-1}$. From the previously determined size of the anatase nanocrystallites,[1] $d = 9$ ± 1 nm at 350 °C, and, assuming that the anatase crystallites are spherical, the corresponding specific surface area can be estimated as follows:

$$S_{Sp} = \frac{6}{\rho_{anatase} \times d}$$

The calculated value is equal to 175 ± 20 $m^2 \cdot g^{-1}$ which is very close to the measured one, in agreement with an accessibility of the nitrogen probe on the major part of the surface of the anatase crystallites. These values are both significantly larger than the theoretical specific surface area calculated for an ideal 2D hexagonal structure with smooth cylindrical pores and dense titania walls (65 $m^2 \cdot g^{-1}$).

Figure 7a shows the evolution of a 1D-XRD pattern of samples PX treated at 350 °C as a function of the volume fraction of surfactant, $\Phi_V(P_{123})$. Figure 7b reports the evolution, versus $\Phi_V(P_{123})$, of the intensity of

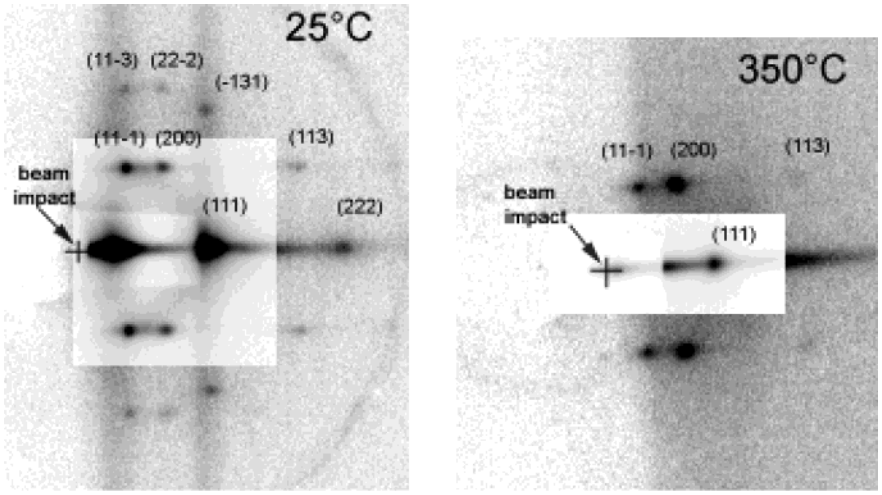

Figure 9. 2D-XRD patterns of layer F67: (a) dried at 25 °C, and (b) calcined at 350 °C.

the main XRD peak. This curve exhibits a maximum for the composition P70. It must be noted that no significant evolution, versus composition, of the layer thickness has been observed. On the other hand, the domain of composition giving rise to ordered layers is located between $\Phi_V = 60\%$ and $\Phi_V = 75\%$, in the center of the 2D hexagonal domain in the water−P_{123} binary diagram.[22] Moreover, this range of composition coincides with those previously determined for ordered silica and alumina layers (Figure 7b).[20,29,32]

Thin Layers of FX Type. To prepare mesoporous layers with a cubic mesostructure, the triblock copolymer P_{123} was replaced by the compound F_{127}, which is known to form a bicontinuous cubic mesophase (space group *Im*3*m*) in the central part of the water−F_{127} binary diagram.[22]

As previously shown with the samples P70, the ordered mesostructure of the layers F67 ($\Phi_V(F_{127}) = 67\%$) is maintained until 500 °C (Figure 8). In that case, a very weak shift of the main XRD peak is evidenced during calcination; the shrinkage of the inorganic network is not so important.

The 2D-XRD patterns of sample F67 treated at 25 and 350 °C confirm the cubic nature of the mesostructure (Figure 9). However, the indexation cannot be made on the basis of the expected space group *Im*3*m* but with the space group *Fm*3*m* encountered for a face-centered cubic close-packing of spherical entities.[42] The AFM observations on the surface of the layer do not allow evidence of an ordered structure (Figure 4b). Such images have been previously obtained for mesoporous silica samples synthesized from micellar cubic mesophases.[43,44] TEM observations are shown in Figure 5c.

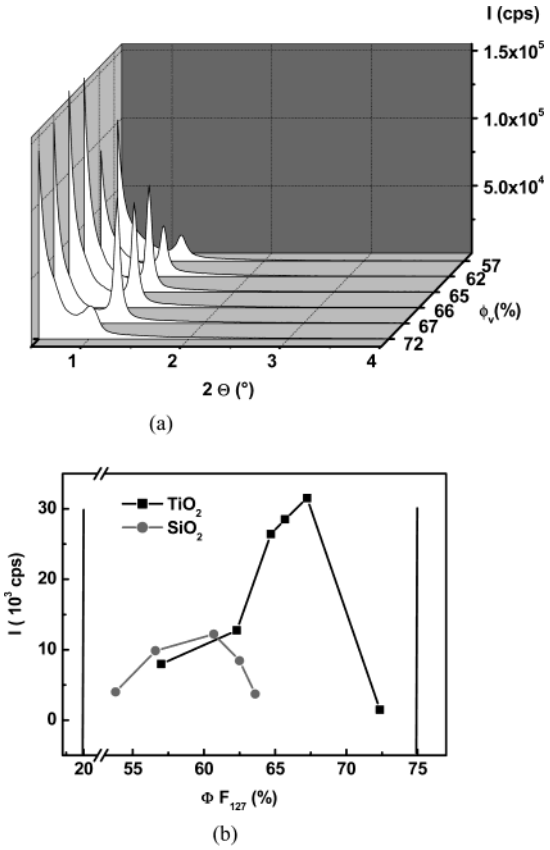

Figure 10. (a) Low-angle 1D-XRD pattern evolution versus Φ_V (F_{127}) for layers FX; and (b) evolution of the intensity of main diffraction peak as a function of Φ_V (F_{127}). The limits of the cubic phase at 30 °C in the water−F_{127} binary diagram are reported as vertical lines.

It is here possible to visualize a cubic arrangement. The images look like those obtained with cubic mesoporous silica.[38,44] The distance between the centers of pores, 9 ± 1 nm, is in agreement with the distance deduced from the 1D X-ray diffraction measurements, 8.5 ± 0.5 nm. The pore diameter estimated by TEM is equal to 4 ± 1

(36) Klotz, M.; Albouy, P. A.; Ayral, A.; Menager, C.; Grosso, D.; Van der Lee, A.; Cabuil, V.; Babonneau, F.; Guizard, C. *Chem. Mater.* **2000**, *12*, 1721.
(37) Langford, J. I.; Wilson, A. J. C. *J. Appl. Cryst.* **1978**, *11*, 102.
(38) Yamada, T.; Zhou, H.-S.; Uchida, H.; Tomita, M.; Ueno, Y.; Ichino, T.; Honma, I.; Asai, K.; Katsube, T. *Adv. Mater.* **2002**, *14*, 812.
(39) Lowell, S.; Shields, J. E. *Powder Surface Area and Porosity*; Chapman and Hall: London, 1984.
(40) Zhao, D.; Yang, P.; Melosh, N.; Feng, J.; Chmelka, B. F.; Stucky, G. D. *Adv. Mater.* **1998**, *10*, 1380.
(41) Ravikovitch, P. I.; Neimark, A. V. *Langmuir* **2002**, *15*, 1550.
(42) Lisiecki, I.; Albouy, P. A.; Pileni, M.-P. *Adv. Mater.* **2003**, *15*, 712.
(43) Paik, J.-A.; Kitazawa, N.; Fan, S.-K.; Kim, C.-J.; Wu, M. C.; Dunn, B. *Mater. Res. Soc. Symp. Proc* **2000**, *657*.
(44) Kim, J. M.; Sakamoto, Y.; Hwang, Y. K.; Kwon, Y.-U.; Terasaki, O.; Park, S.-E.; Stucky, G. D. *J. Phys. Chem. B* **2002**, *106*, 2552.

nm. From the nitrogen adsorption−desorption isotherm (Figure 6b), the mean spherical pore diameter[41] determined by the BJH method applied on the adsorption branch is 4.8 ± 0.2 nm, in agreement with the TEM value. The BET surface is equal to 180 $m^2 \cdot g^{-1}$which is close to the values measured or calculated for sample P70.

Ordered anatase layers FX are obtained for a volume fraction of F_{127} ranging from 55 to 70%, (Figure 10a). A weak shift to the larger volume fractions is observed in comparison with the range of composition giving rise to mesostructured silica layers[20] (Figure 10b).

Conclusions

This study enables us to specify the mesostructure of anatase thin films prepared by templating mesophases from two triblock copolymers, P_{123} and F_{127}. With P_{123}, thin films with an anisotropic and distorted 2D hexagonal mesostructure are obtained in accordance with the mesophase structure expected from the water−P_{123} phase diagram. The unidirectional shrinkage of the layer in the direction of the normal of the film gives rise to the deformation of the 2D hexagonal planar geometry *p*6*mm* into a planar rectangular geometry, *c*2*mm*. In the case of F_{127}, the obtained cubic mesostructure (geometry *Fm*3*m*) corresponds to that usually observed for face-centered cubic arrangements of spherical micelles and not to the expected geometry referring to the bicontinuous cubic mesophase (*Im*3*m*) evidenced in the water−F_{127} binary diagram. It can be noted that such discrepancy between the structure of the mesophases formed in pure water and that of mesophase-templated layers has been previously demonstrated in other cases such as in the silica−CTAB system.[45]

Studies are now in progress to compare the two types of mesostructured anatase layers in terms of gas and liquid permeability and of photocatalytic properties.

Acknowledgment. We thank A. El Mansouri (I.E.M., Montpellier, France), Arie van der Lee (I.E.M., Montpellier, France), and M. Klotz (St Gobain Recherche, Paris, France) for their help with the nitrogen adsorption−desorption, 1D-XRD, and AFM characterizations, respectively.

CM049893A

(45) Besson, S. Films organisés de silice mésoporeuse: synthèse, caractérisation structurale et utilisation pour la croissance de nanoparticules, Ph.D. Thesis, Ecole Polytechnique, Paris, France, 2002.